Med Biol Eng Comput (2015) 53:771–780
DOI 10.1007/s11517-015-1287-6

ORIGINAL ARTICLE

Continuous-wavelet-transform analysis of the multifocal ERG waveform in glaucoma diagnosis

J. M. Miguel-Jiménez[1] · R. Blanco[1] · L. De-Santiago[1] · A. Fernández[1] · J. M. Rodríguez-Ascariz[1] · R. Barea[1] · J. L. Martín-Sánchez[1] · C. Amo[1] · E. Sánchez-Morla[1] · L. Boquete[1]

Received: 16 July 2013 / Accepted: 26 March 2015 / Published online: 8 April 2015

Abstract The vast majority of multifocal electroretinogram (mfERG) signal analyses to detect glaucoma study the signals' amplitudes and latencies. The purpose of this paper is to investigate application of wavelet analysis of mfERG signals in diagnosis of glaucoma. This analysis method applies the continuous wavelet transform (CWT) to the signals, using the real Morlet wavelet. CWT coefficients resulting from the scale of maximum correlation are used as inputs to a neural network, which acts as a classifier. mfERG recordings are taken from the eyes of 47 subjects diagnosed with chronic open-angle glaucoma and from those of 24 healthy subjects. The high sensitivity in the classification (0.894) provides reliable detection of glaucomatous sectors, while the specificity achieved (0.844) reflects accurate detection of healthy sectors. The results obtained in this paper improve on the previous findings reported by the authors using the same visual stimuli and database.

Keywords Glaucoma · Multifocal ERG · Continuous wavelet transform · Neural network

1 Introduction

The search for novel techniques to monitor ganglion cell function is motivated by the potential for earlier and more precise detection and management of glaucoma. Methods for early detection and mapping of dysfunctional retinal areas provide a more accurate means of identifying people at risk and improve disease management. It is possible that early functional changes are detectable before significant fiber loss occurs and at a stage where these changes may still be reversible through early intervention [33]. It is often stated that structural changes seen by means of techniques such as optical computerized tomography (OCT) and frequency-doubling perimetry (FDP) precede functional changes. This may well be true when these techniques are compared with various methods of psychophysical perimetry [25].

Some studies using FDP showed that, in patients with open-angle glaucoma with established hemifield defects, 41 % of 49 hemifields with apparently normal fields produced abnormal FDP results [35]. Also, several studies using short-wavelength automated perimetry (SWAP) show that this technique may be able to detect visual field defects before Humphrey visual field (HVF) perimetry in cases of suspected glaucoma and may detect earlier progression of visual field defects in glaucoma patients [3].

Alternative approaches to obtaining objective measures of glaucomatous neuropathy which do not rely on psychophysiological or structural testing have also been investigated in recent years. One approach has been use of electroretinograms (ERGs) to measure changes in electrical activity generated by the retinal ganglion cell bodies or axons in glaucoma [12, 13, 17].

Use of ERGs in glaucoma detection requires isolation of specific components related to ganglion cell responses. Research into use of ERGs in experimental glaucoma detection has produced clear support for the suggestion that electrophysiological tools can detect early functional changes in glaucoma [14]. Several studies have

✉ J. M. Miguel-Jiménez
jmanuel@depeca.uah.es

L. Boquete
luciano.boquete@uah.es; luciano@depeca.uah.es

[1] Department of Electronics, University of Alcalá, Alcalá de Henares, Spain

demonstrated that pattern-reversal ERG (PERG) is abnormal in glaucoma [16]. However, a clear limitation of the use of full-field stimuli for flash ERGs and pattern ERGs has been that this type of stimulation does not allow measurement of the localized functional losses seen in early glaucoma.

A potentially more effective procedure is the mfERG [32], which produces simultaneous recordings of focal responses from over 100 different retinal regions to derive topographic representations of retinal response components. Several studies have also provided strong evidence that mfERG responses contain significant contributions generated by inner retinal mechanisms, including ganglion cell action potentials. The most obvious change in the mfERG associated with advancing visual field defects is loss of oscillatory potentials. However, standard-luminance-flicker mfERG responses contain a relatively small ganglion cell contribution, which limits the usefulness of such stimuli for assessment of function in glaucoma [17].

These results have motivated interest in isolating response components related to ganglion cell activity by using novel stimulation protocols in mfERGs. A number of paradigms have been developed to help detect damage to the inner retina (i.e., amacrine and ganglion cells) in mfERGs [6, 11, 29]. Several of these multifocal paradigms—the global flash techniques, which combine multifocal stimulation with periodic 'global' (full-screen) stimuli—are characterized by their ability to extract a larger ganglion cell contribution [31]. These techniques evoke a large nonlinear mfERG component (the induced component, IC). This is an interaction between a focal flash and a periodic global flash that contains contributions from lateral interactions mediated by the inner retinal circuitry. The IC represents effects of local flash responses on periodic full-screen flash responses interleaved between the multifocal stimuli. As this IC contains effects of the focal flash responses on subsequent responses elicited in the same, as well as in surrounding areas, it is believed to reflect properties of ganglion cell receptive fields. It has since been shown that mfERG abnormalities in glaucoma are due to loss of this optic nerve head component (ONHC) [4]. The existence of the ONHC has been well established in humans and in animal models [18].

Most mfERG response studies have been based on simple waveform analyses, such as peak amplitudes and latency measurements [7, 15, 20, 34]. Other papers analyze mfERG signals in the frequency domain [23, 24, 26, 28], or time–frequency analysis, although more complex analyses have been carried out lately to leverage the diagnostic accuracy of the technique [5, 10, 24]. For example, discrete-wavelet-transform (DWT) analysis has been used to detect changes in mfERG signals recorded in patients with advanced open-angle glaucoma using the global flash paradigm [26].

The aim of this study is to classify glaucomatous and healthy sectors based on the frequency content within the mfERG recordings' IC. The differences in their frequency content are easily detected using the Morlet wavelet transform. In this paper, we study potential application of the CWT as a means of identifying significant changes in the mfERG recordings' IC. This time interval is the most affected in glaucoma analysis and also offers a more precise and reliable means of discriminating between normal and abnormal mfERG waveform signals in optic nerve diseases.

The two-global-flash mfERG (MFOFO) paradigm protocol used in this study provides a reliable and objective measure of visual loss in glaucomatous patients. This stimulation paradigm extracted a large ONHC contribution from the mfERG responses, thereby making it easier to detect waveform abnormalities.

2 Methods

2.1 Subject database

The database used in this paper is composed of two groups: glaucomatous mfERG signal recordings taken from the eyes of 47 subjects (29 males and 18 females) diagnosed with chronic open-angle glaucoma, and those taken from 24 control subjects (12 males and 12 females). All subjects were between 40 and 60 years old, and all were assessed by the Department of Ophthalmology at the University of Alcalá (Spain). Mean ages were 47.5 (SD $\pm$ 2.5) in the control group and 50.7 (SD $\pm$ 3.8) in the glaucoma group.

Each subject underwent a comprehensive ophthalmologic examination, including review of his/her medical history, measurement of best-corrected visual acuity, slit-lamp biomicroscopy, measurement of intraocular pressure using Goldmann applanation tonometry, dilated fundoscopic examination and automated perimetry using the 24-2 Swedish interactive threshold algorithm (Carl Zeiss Meditec, Inc). Informed consent was obtained from all participants. The University of Alcalá approved all the protocols, and the study was conducted in accordance with the tenets of the Declaration of Helsinki.

2.2 Procedure overview

Figure 1 shows the block diagram for the mfERG signal analysis process. It is structured into the following phases:

- Two-global-flash multifocal stimulation (Fig. 1a) and signal capture (Fig. 1b).

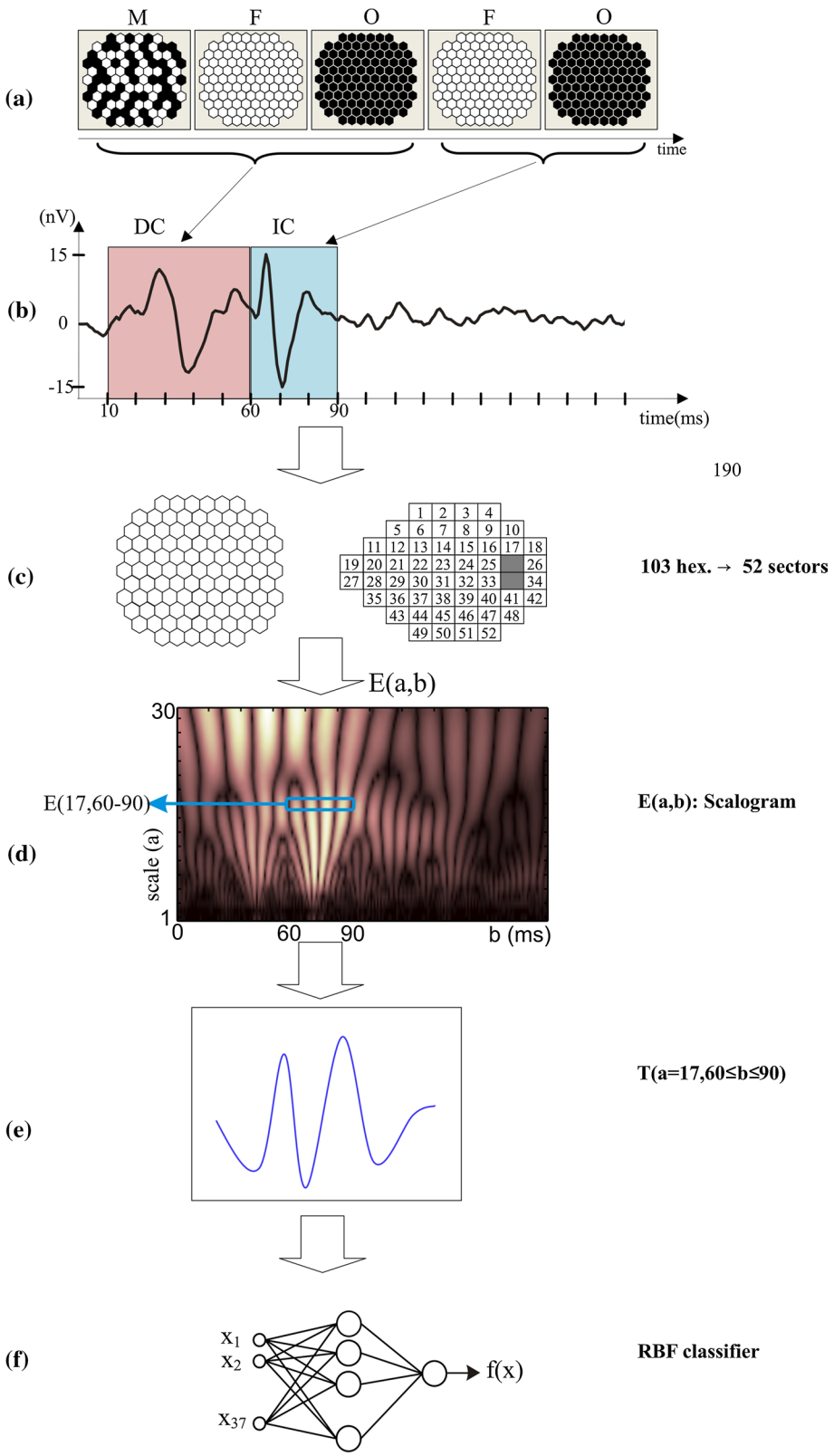

Fig. 1 **a** Two-global-flash MfERG stimulation. **b** The responses are formed by two consecutive components: the direct component (10–60 ms interval) and the indirect component (60–90 ms). **c** mfERG responses were regrouped to create a new 52-sector map similar to the standard 24-2 HVF. **d** Application of the CWT to the signal's IC. **e** Extraction of the coefficients resulting from the CWT's a_{max} scale. **f** RBFN used to classify the recording as either glaucomatous or healthy

- Conversion of 103 hexagons (mfERG topographic map) into 52 sectors to compare the mfERG signal maps with the HVF (Fig. 1c).
- Application of the CWT to the signal's IC (Fig. 1d).
- Extraction of the coefficients resulting from the CWT's a_{max} scale (Fig. 1e).

- The CWT's a_{max} scale coefficients serve as input vectors to a radial-basis-function network (RBFN) used to classify the recording as either glaucomatous or healthy (Fig. 1f).

2.3 mfERG acquisition

All patient recordings were taken using a commercially available multifocal system (VERIS System 5.1, Electro-Diagnostic Imaging, Inc., San Mateo, CA). The stimulus (Fig. 1a) consisted of an array of 103 densely packed hexagons tiling the central region of the visual field and about 45 degrees in diameter. The hexagonal stimulus elements were eccentrically scaled to equalize, approximately, the response amplitudes across the stimulated field (stretch factor of 10.46). The stimulus array was presented on a 21-inch monochrome CRT monitor (NEC-FE2111SB) at a video frame rate of 75 Hz. The eyes were kept light-adapted at room illumination prior to recording. The stimulus was viewed through pharmacologically dilated pupils, and a Burian-Allen bipolar contact lens electrode was placed on the eye.

Some studies have already shown that interposing bright global flashes into the stimulation sequence increases the inner retinal contributions to the mfERG and therefore its sensitivity in glaucoma detection [28]. In the present study, two-global-flash mfERG stimulation was used. Each step of the ganglion cell response-enhancing stimulation protocol (MFOFO) consisted of five video frames (Fig. 1a). In the first frame (M), each stimulus hexagon was either independently flashed (200 cd/m^2) or remained dark (<1.5 cd/m^2) according to a pseudorandom binary m-sequence. The second and fourth frames (F) contained global flashes (100 cd/m^2), and the third and fifth (O) were dark (<1.5 cd/m^2).

Signals were amplified with a Grass Neurodata Model 12 amplifier system with a gain of 50,000, band-pass filters (10–300 Hz) and a sampling interval of 0.83 ms (1200 Hz). The responses had a duration of 190 ms and were formed by two consecutive components (Fig. 1b): the direct component (DC) located at the start of the recording (10–60 ms) and the IC defined in the 60–90-ms time interval. The IC represents a large nonlinear mfERG component, which is an interaction between a focal flash and a periodic global flash that contains contributions from lateral interactions mediated by the inner retinal circuitry. As this IC contains effects of the focal flash responses on subsequent responses elicited in the same, as well as in surrounding areas, it is believed to reflect properties of ganglion cell receptive fields.

2.4 mfERG processing

To compare visual field sensitivity and mfERG responses, the signals of each eye's 103 hexagons were regrouped. In the cases in which more than one mfERG signal coincided, these were averaged to create a new 52-sector map similar to the standard 24–2 HVF (Fig. 1c). We used the third approach presented in [19] to determine the relationship between visual fields and multifocal responses. This approach estimates the thresholds for the multifocal display's regions by interpolating values at the standard Humphrey locations.

Abnormal mfERG signals from glaucomatous patients were selected based on their spatial coincidence with abnormal sectors in the HVF test (defined by a consistent loss of sensitivity of over 10 dB in at least two repeated visual field tests). An abnormal HVF result was characterized by a pattern standard deviation (PSD) and/or corrected pattern standard deviation (CPSD) below the 95 % CI, or by a glaucoma hemifield test (GHT) result outside the normal limits. A test was considered unreliable if false positives, false negatives or fixation losses exceeded 33 %.

A total of 1374 glaucomatous and control sectors were selected for each database. Half the recordings in each group (687) were selected at random to train the neural networks, while the other half was used to validate analysis.

SPSS software, version 13 (SPSS Inc., Chicago, IL, USA) was used for statistical analysis. Statistical significance was assumed at $p < 0.05$. Multiple sectors from the same subjects were included in both the training and validation data sets. Due to this sample dependence, the most suitable test for correlated observations was used (Wilcoxon signed-rank test), as stated in previous papers [30].

2.5 Wavelet signal analysis

The mfERG signals were analyzed using the continuous wavelet transform. The wavelet transform of a continuous time signal, $x(t)$, is defined as:

$$T(a,b) = \frac{1}{\sqrt{a}} \int_{-\infty}^{+\infty} x(t)\Psi^*\left(\frac{t-b}{a}\right)\mathrm{d}t \quad (1)$$

where $\Psi^*(t)$ is the complex conjugate of wavelet function $\Psi(t)$; a is the dilation parameter of the wavelet; and b is the translation parameter. Wavelet function $\Psi(t)$ should fulfill the following conditions:

(i) It must have finite energy: $E = \int_{-\infty}^{+\infty} |\Psi(t)|^2 \mathrm{d}t < \infty$.

(ii) It must have a zero mean (admissibility condition).

(iii) For complex (or analytic) wavelets, the Fourier transform ($\Psi(\omega)$) must both be real and vanish for negative frequencies.

Wavelet transform $T(a, b)$ is a bi-dimensional function that shows the correlation (inner product) between the

signal, $x(t)$, and the wavelet function at different scales (a) and time instants (b). Wavelet analysis can specify the frequency characteristics of a signal at any given time. In other words, wavelet analysis is well suited to discriminating signals whose frequency components change over time. Wavelet analysis has demonstrated its utility in numerous signal-processing applications in biomedical engineering [1, 10].

In this paper, the real Morlet wavelet is used as the wavelet function:

$$\Psi(t) = e^{-\frac{t^2}{2}} \times \cos(\omega_0 t) = e^{-\frac{t^2}{2}} \times \cos(5t) \tag{2}$$

The module of the Fourier Transform of the real Morlet wavelet function is as follows:

$$|\Psi(\omega)| = \sqrt{\pi} \times e^{-\frac{(\omega-\omega_0)^2}{2}} \tag{3}$$

Its spectral response centers on ω_0. Its bandwidth is defined by the following expression:

$$\omega_{3\mathrm{dB}} = \omega_0 \pm \sqrt{2 \times \ln\sqrt{2}}.$$

It should be noted that the real Morlet function (Eq. 2) does not strictly fulfill the condition of having a null mean value (ii), although its value is close to zero:

$$|\Psi(\omega = 0)| = 6.6 \times 10^{-6} \cong 0 \tag{4}$$

The scalogram is the squared magnitude of the wavelet transform [9] and represents contribution to signal energy at a specific scale (a) and position (b):

$$E(a,b) = |T(a,b)|^2 \tag{5}$$

The scale of maximum correlation ($a_{\max}$) of transform $T(a, b)$ is defined as the value for which, at given position b_o, the following is fulfilled: $|E(a_{\max}, b_0)| \geq |E(a,b)|$. $a_{\max}$ corresponds to the scale in which the maximum correlation value appears between the signal, $x(t)$, and the wavelet function, and may be used for locating and characterizing singularities in signal $x(t)$.

As sampled signals are used, the sampling frequency and its relationship with the wavelet frequency should be taken into consideration. If sampling frequency f_s is used, central frequency f_a of an a-scale wavelet would be as follows:

$$f_a = \frac{f_s \omega_0}{2 \times \pi \times a} \tag{6}$$

The CWT was applied to each of the 52 sectors in the $60 < b < 90$ ms time interval for scales $1 \leq a \leq 100$. Repeated testing with some wavelets (Daubechies 6, Biorthogonal 3.1 and real Morlet) showed that the real Morlet wavelet obtained the highest correlation value in the function $E(a, b)$ within the healthy recordings' complete interval (0–190 ms) and for a 1–100 scale range. That is why real Morlet wavelet was decided to use in this paper. Once $T(a, b)$ is obtained for a sector, scale $a_{\max} = 17$ of the same is selected. This is approximately equivalent to using a band-pass filter centered on 56.20 Hz with cutoff frequencies at 65.50 and 46.80 Hz.

2.6 RBFNs as classifiers

Neural networks' example-based learning capacity makes them suitable for use as classifiers. RBFNs offer simple architecture and high generalization capacity. An RBFN consists of input, hidden (N_H) and output nodes. Each neuron in the single hidden layer corresponds to a basis function, exp(.), activated by the distance between an input vector ($\mathbf{X}$) and the center of the basis function ($\boldsymbol{\mu}_i$). The output of the network is a linear combination of the basis functions:

$$f(X) = \sum_{i=1}^{N_H} w_i \cdot e^{-\frac{|X-\mu_i|^2}{\sigma_i^2}} = \sum_{i=1}^{N_H} w_i \cdot g_i(X) \tag{7}$$

where w_i denotes the output weight matrix and σ_i is the width of the basis function. An RBFN is a three-layer network that is linear with respect to the output parameters if the rest of the parameters are fixed: N_H, σ_i and $\boldsymbol{\mu}_i$.

The neuron layer performs nonlinear transformation and maps the input space onto a new space. The output layer implements a linear combiner on this space, where the adjustable parameters are the weights w_i. Various methods may be used to adjust the $\mathbf{W}$ weight matrix [36]. In this paper, the gradient descent algorithm is used. If $f(\mathbf{x})$ is the actual output and $fd(x)$ is the desired output for input x, the error is defined as:

$$E = \frac{1}{2}\left[f(\mathbf{x}) - f_d(\mathbf{x})\right]^2 \tag{8}$$

and w_i weight adjustment is:

$$\Delta w_i = -\alpha \times \frac{\partial E}{\partial w_i} = -\alpha \times (f(x) - f_d(x)) \times g_i(x); \quad \alpha > 0 \tag{9}$$

As signal morphology depends on the position that the sector under study occupies on the retina [5], a neural network was trained for each sector into which the retina was divided (i.e., 52 RBFNs in total) in order to classify the recordings. The coefficients obtained in transform $T(a, b)$ in scale $a = 17$ and in the IC window were used as input vectors to the neural network: $T(17, 60 \leq b \leq 90)$. The reason for choosing the coefficients within $T(17, 60 \leq b \leq 90)$ was to optimize the classification capacity (as explained in '*Selection of the optimal* $a_{\max}$ *value*'). As the analog signals' sampling frequency was 1200 Hz, the number of elements in each input vector was $(0.09–0.06) \times 1200 + 1 = 37$.

The 52 neural networks used share the following common architecture: number of inputs = 37; number of N_H neurons = 22 (uniform distribution of the μ_i centers in the input space); desired outputs = +1 (glaucomatous sector), −1 (healthy sector); gradient descent algorithm ($\alpha = 0.1$); and decision threshold = 0.0.

To train the neural networks, half of the recordings in the database were used (i.e., 687 recordings of healthy control sectors and 687 recordings of glaucomatous sectors). Because each patient with glaucoma had a different number of affected sectors, recordings from different numbers of patients could contribute to each sector in the database. The minimum and maximum numbers of sectors per patient were 14 and 37, respectively (SD = 7.6). Glaucomatous sectors 1 and 2 had the least number of contributing recordings (4 each), and sector 20 had the highest (44). This means that 2 healthy sectors + 2 glaucomatous sectors were used to train the neural network with the least number of sectors, and the same number was used for validation. For the RBFN associated with sector 20, 22 healthy sectors + 22 glaucomatous sectors were used in training and validation.

3 Results

Figure 2 shows the scalograms of mfERG recordings taken of two sectors—a glaucomatous sector (Fig. 2a) and an unaffected sector (Fig. 2b). Both cases display function $E(a, b)$ in the recordings' complete interval (0–190 ms) and for a 1–100 scale range. The scalograms in Fig. 2 show the energy distribution in the time–scale plane.

Figure 3a shows the scale in which the maximum value of $E(a, b)$ is found within the IC window and for each of the groups of recordings analyzed (687 healthy and 687 glaucomatous). Figure 3b represents the time instant in

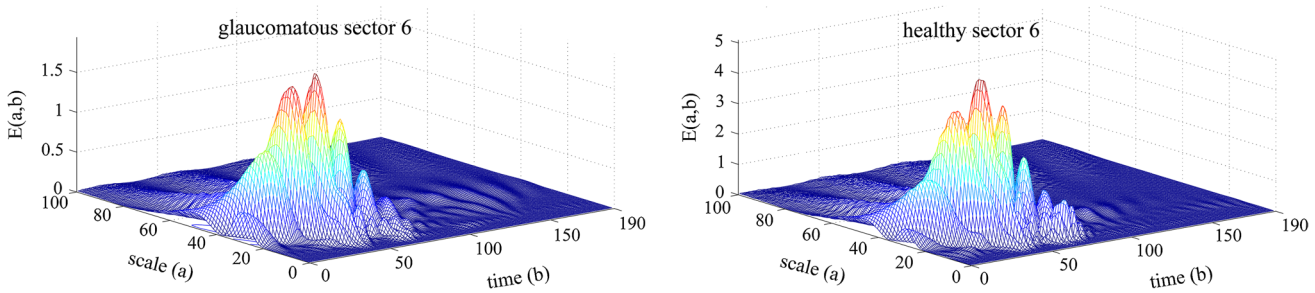

Fig. 2 3D representation of $E(a, b)$ ($0 < b < 190$ ms, $1 \leq a \leq 100$). **a** $E(a, b)$ of sector 6 affected by glaucoma. **b** $E(a, b)$ of sector 6 in a healthy eye

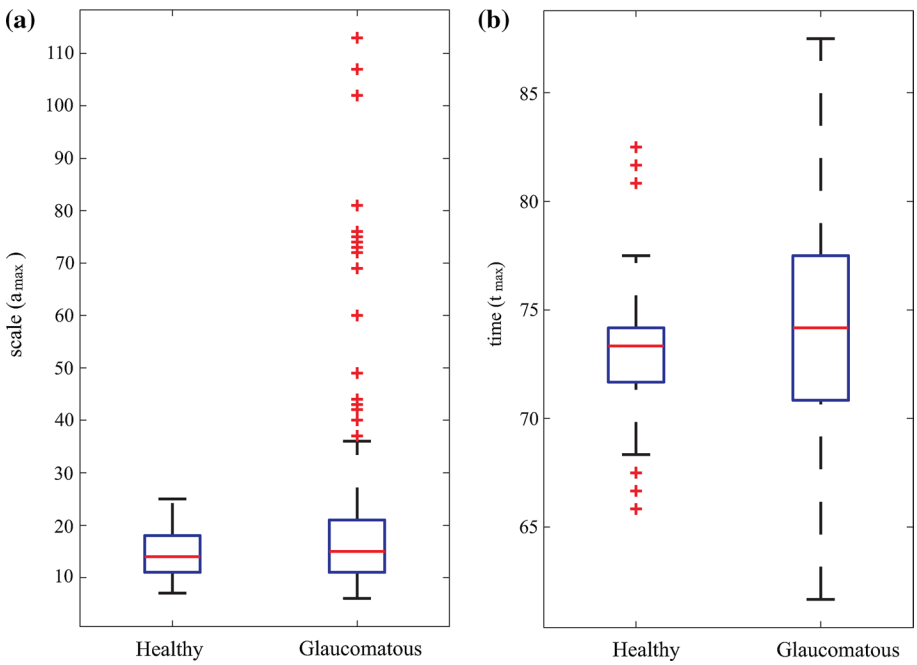

Fig. 3 **a** Distribution of scale a_{max} for healthy and glaucomatous sectors. For healthy sectors, the mean value of the maximum scale is 13.91 (SD ± 3.96), and for glaucomatous sectors, it is 17.76 (SD ± 10.99). **b** Time instant of presence of a_{max} within the IC. The respective values for healthy and glaucomatous recordings are 72.46 ms (SD ± 2.82) and 74.20 ms (SD ± 4.46)

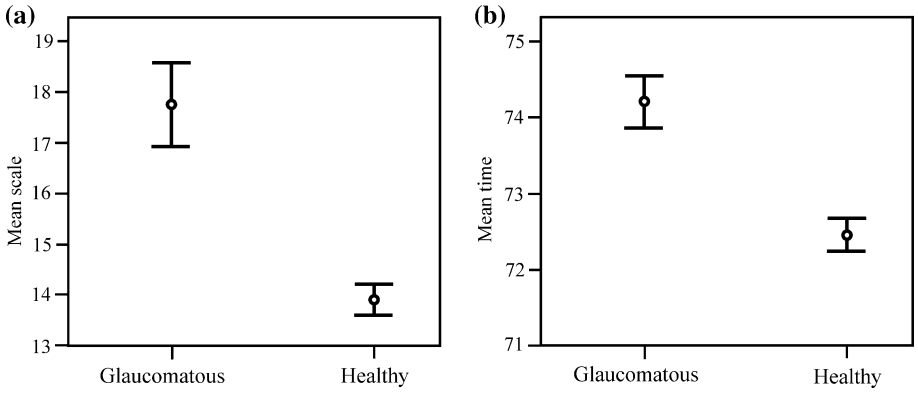

Fig. 4 **a** Mean and 95 % CI for time in both groups (healthy and glaucomatous). **b** Mean and 95 % CI for the scales

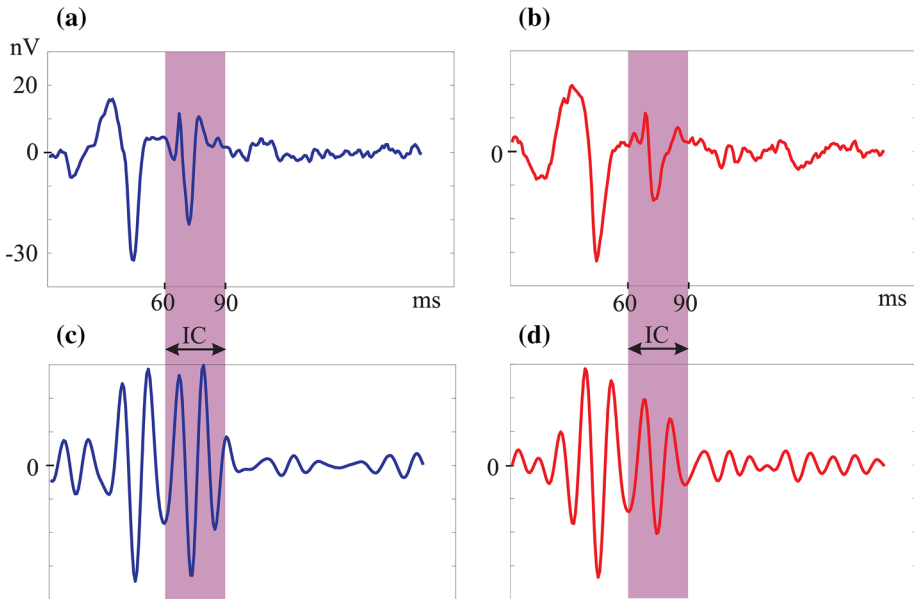

Fig. 5 Analysis of the signal associated with sector 6 in one eye of a healthy control subject and in one eye of a subject affected by glaucoma in the same sector. **a** Multifocal signal of the healthy sector. **b** Multifocal signal of the sector affected by glaucoma. **c** Value of all the wavelet coefficients in scale $a = 17$ obtained from recording (**a**). **d** Value of the CWT coefficients in scale $a = 17$ obtained from recording (**b**)

which the above-mentioned maximum value appears (b_0). These figures depict both groups through their quartiles, whiskers (indicating variability outside the upper and lower quartiles) and outliers, plotted as individual points.

For the healthy sectors, the mean value of the maximum scale is 13.91 (SD ± 3.96) and the value is always below 25. For the glaucomatous recordings, the mean value of the scale is 17.76 (SD ± 10.99), with recordings containing maximums of up to scale 113 being found. The primary difference is that there is a greater spread of values in the glaucomatous sectors as these signals have more irregular forms.

As regards the time instant in which maximum correlation is produced (always within the signal's IC interval), the respective values for the healthy and glaucomatous recordings are 72.46 ms (SD ± 2.82) and 74.20 ms (SD ± 4.46). These results can be justified because the healthy signals have a predictable morphology, while the morphology of the glaucomatous sectors' signals is more chaotic, which is reflected in the wider spread of b_0 values.

Figure 4a shows the mean and the 95 % CI for the time in both groups, while Fig. 4b shows the same for the scales. A statistically significant difference has been noted in scale (a_{max}) values ($p < 0.001$) and in time (t_{max}) values ($p < 0.001$) according to the Wilcoxon signed-rank test.

Figure 5 shows the result of correlation between two recordings taken of sector 6 (one healthy one and another glaucomatous one) and the Morlet wavelet in scale $a = 17$. The 37 CWT coefficients corresponding to the IC window within scale 17 (Fig. 5c, d) form the input vector used to train the specific neural network for each of the 52 sectors.

3.1 Selection of the optimal a_{max} value

Scale a_{max} is used to obtain the coefficients, which are also used as the inputs to the neural classifier. In order to

determine the optimal a_{max} value, tests of the entire method shown in Fig. 1 were carried out on various a_{max} values. The ultimate objective of the classification process is to obtain the best sensitivity (Se) and specificity (Sp) values. The analyzed sectors were used as the training set for the neural networks, and the validation group was used as the test set. Table 1 summarizes the results obtained for values $10 \leq a_{max} \leq 20$.

To determine the best discrimination scale between the two groups of recordings (healthy and glaucomatous), the minimum distance between the points (Se, 1 − Sp) on the receiver operating characteristic (ROC) plane and point (0, 1)— perfect classifier— were used [22]:

$$d = \sqrt{(1 - \mathrm{Se})^2 + (1 - \mathrm{Sp})^2} \tag{10}$$

Note that Eq. 10 gives equal weight to sensitivity and specificity and imposes no ethical cost and no prevalence constraints. According to these criteria, the most appropriate maximum correlation scale is $a_{max} = 17$ (Table 1).

3.2 Classification

The contingency table (Table 2) shows the results of classifying the validation recordings, composed of the same number of sector recordings as when performing training (i.e., 687 healthy control sectors and 687 glaucomatous sectors) and using $a_{max} = 17$.

According to the results shown in Table 2, 89.4 % of the glaucomatous recordings were detected as such, while in the group of healthy recordings 84.4 % were detected accurately.

In this study, the positive predictive value (PPV), i.e., the proportion of correctly diagnosed patients with positive test results, was 0.852. The negative predictive value (NPV), i.e., the proportion of correctly diagnosed patients with negative test results, was 0.888 [2]. However, calculating the predictive values based on the contingency table has the disadvantage that these values depend on the proportion of glaucomatous subjects in the sample studied. It is therefore necessary to establish other assessment indices that are both clinically useful and independent of the proportion of glaucomatous subjects in the sample. Consequently, the positive (CP^+) and negative (CP^-) probability ratios are used. These measure how much more probable a specific positive or negative result is according to the presence or absence of disease.

Values greater than CP^+ ($CP^+ = \frac{Se}{1-Sp}$) indicate a better capacity to diagnose the presence of disease (5.738 in our results), while values less than CP^- ($CP^- = \frac{1-Se}{Sp}$) indicate a better capacity to confirm the absence of disease ($CP^- = 0.126$).

Table 1 Results of classification for various scale values

Scale (a)	Central frequency (Hz)	Sensitivity (Se)	Specificity (Sp)	$\boldsymbol{d = \sqrt{(1 - Se)^2 + (1 - Sp)^2}}$
10	95.54	0.836	0.837	0.232
11	86.86	0.824	0.853	0.229
12	79.62	0.847	0.846	0.217
13	73.49	0.841	0.863	0.210
14	68.24	0.857	0.836	0.218
15	63.69	0.868	0.854	0.197
16	59.71	0.873	0.852	0.195
17	**56.20**	**0.894**	**0.844**	**0.189**
18	53.08	0.860	0.877	0.190
19	50.28	0.838	0.871	0.207
20	47.77	0.846	0.866	0.204

The central frequency of each scale is also indicated (calculated using Eq. 6)

Bold indicates the scale at which the maximum correlation appears

Table 2 Contingency table CWT and RBFN–HVF (value $p < 0.0001$)

	Glaucomatous HVF	Healthy HVF	
Glaucomatous CWT and RBFN	614 sectors	107 sectors	PPV = 0.852 $CP^+ = 5.738$
Healthy CWT and RBFN	73 sectors	580 sectors	NPV = 0.888 $CP^- = 0.126$
	Sensitivity = 0.894	Specificity = 0.844	

Sensitivity, specificity, PPV, NPV, CP^+ and CP^-

4 Discussion

The principal purpose of this paper is to develop a new mfERG signal analysis method using the continuous wavelet transform and a neural network as a classifier. The ultimate objective is to classify as either healthy or glaucomatous the various sectors into which the patient's retina is divided.

The most important finding of this paper is the ability to differentiate between normal and glaucomatous recordings based on the frequency content within the IC. Wavelet analysis revealed that the scale of maximum correlation for healthy sectors was $a_{max} = 13.91$ (SD $\pm$ 3.96). This is equivalent to stating that the maximum frequency response, within the signal's IC interval, is 68.69 Hz (SD $\pm$ 15.22 Hz). In none of the healthy sectors was $a_{max} > 25$ (38.22 Hz).

For glaucomatous sectors, the maximum correlation within the IC interval was produced at $a_{max} = 17.76$ (SD $\pm$ 10.99), which in the frequency domain is equivalent to 53.80 Hz (SD $\pm$ 20.35 Hz). The study found glaucomatous sectors with a scale of maximum correlation of $a_{max} = 113$ (8.45 Hz).

As an initial justification of the results obtained, it may be stated that healthy signals generally have a predetermined morphology. Therefore, the spread of the a_{max} value is less than in glaucomatous signals, for which the waveform, and therefore its representation in the frequency domain, is more arbitrary.

To identify the optimal a_{max} value, the criterion selected was that of closest distance to the (0, 1) point, the value obtained being $a_{max} = 17$. Using the database available, this value makes it possible to optimize the classification capacity of the complete method shown in Fig. 1.

Table 2 shows the results obtained in this study. The high sensitivity (0.894) provides reliable detection of glaucomatous sectors, while the specificity achieved (0.844) reflects accurate detection of healthy sectors. The number of false positives detected (107) suggests that the method proposed could detect glaucomatous defects that the HVF test does not yet consider (sectors that show a loss that is close to but does not exceed 10 dB).

The PPV obtained (0.852) indicates it is highly probable that if the method proposed detects glaucomatous defects, then the subject does indeed present the disease. At the same time, the NPV (0.888) makes the assessment method robust in cases in which the subject does not present the disease. Discrimination between the two groups is significant (Wilcoxon signed-rank test, $p < 0.05$).

The results obtained in this paper improve on the previous findings reported by the authors using the same visual stimuli and database. In [27], sensitivity = 0.81 and specificity = 0.73 values were obtained using wavelet packet decomposition as the mfERG-recording analysis tool. Analyzing 13 of the signals' morphological characteristics and then classifying them using a radial-basis-function-type neural network trained using the Extreme Learning Machine algorithm [5] obtained the following values: sensitivity = 0.853 and specificity = 0.809. Using the discrete wavelet transform [26] as the analysis tool, and also applying it to the signal's IC interval, obtained the following values: sensitivity = 0.845 and specificity = 0.842. Re-applying the criteria described in Eq. 10 reveals that the method presented in this paper is the most effective way of precisely detecting glaucomatous sectors when analyzing mfERG signals.

Our results are consistent with previous studies using alternative techniques such as nerve-fiber-layer thickness analysis [21], FDP [35], SWAP [8] and multifocal visual-evoked potentials [18]. Overall, these results are consistent with the concept that subtle visual field and optic disk damage can be detected if a more sensitive diagnostic tool is available. Studies of nerve-fiber-layer thickness have shown that glaucomatous damage can be present in the visual field hemifield at normal achromatic sensitivity [21].

One limitation of this study is that for some of the sectors into which the retina is divided, there are very few examples with which to train the corresponding neural network. Likewise, selection of the neural-network-based classifier has not been explored in depth (network architecture, alternative training algorithms, etc.) to obtain the best possible results. Another limitation of this study is that multiple sectors from the same subjects are included in both the training and validation data sets, so the independence assumption could be somewhat limited.

5 Conclusions

A high-sensitivity and high-specificity predictive model for detecting early glaucomatous changes in patients with glaucoma was designed. CWT analysis applied to the global flash mfERGs provided an alternative and potentially more accurate method of assessing glaucoma. Further improvement by isolating the ONHC from the mfERGs may increase its diagnostic value in clinical practice.

Acknowledgments This research has been partially supported by the Ministerio de Ciencia e Innovación (Spain) under the program entitled "Advanced Analysis of Multifocal ERG and Visual-Evoked Potentials Applied to Diagnosis of Optic Neuropathies," reference number TEC2011–26066, and by FIS PI11/00533 and RETICS RD12/0034/0006 Granted to R. Blanco.

Conflict of interest The authors claim no conflicts of interest.

References

1. Addison PS (2005) Wavelet transforms and the ECG: a review. Physiol Meas 26:R155–R199
2. Altman DG, Bland JM (1994) Statistics notes: diagnostic tests 2: predictive values. Br Med J 309(102):1
3. Bayer AU, Erb C (2002) Short-wavelength automated perimetry, frequency doubling technology perimetry and pattern electroretinography for prediction of progressive glaucomatous standard visual field defects. Ophthalmology 109:1009–1017
4. Bearse MA, Sutter EE, Stamper RL (2001) Detection of glaucomatous dysfunction using a global flash multifocal electroretinogram (mERG) paradigm. In: Sawchuk A (ed) Vision science and its applications. OSA technical digest series, vol 1. Optical Society of America, Washington, DC, pp 14–17
5. Boquete L, Miguel-Jiménez JM, Ortega S, Rodríguez-Ascariz JM, Pérez-Rico C, Blanco R (2011) Multifocal electroretinogram diagnosis of glaucoma applying neural networks and structural pattern analysis. Expert Syst Appl 39:234–238
6. Chu PH, Chan HH, Brown B (2006) Glaucoma detection is facilitated by luminance modulation of the global flash multifocal electroretinogram. Invest Ophthalmol Vis Sci 47:929–937
7. Chu PH, Chan HH, Brown B (2007) Luminance-modulated adaptation of global flash mfERG: fellow eye losses in asymmetric glaucoma. Invest Ophthalmol Vis Sci 48:2626–2633
8. Delgado MF, Nguyen NT, Cox TA et al (2002) Automated perimetry: a report by the American Academy of Ophthalmology. Ophthalmology 109:2362–2374
9. Delprat N, Escudié B, Guillemain P, Kronland-Martinet R, Tchamitchian P, Torrésani B (1992) Asymptotic wavelet and Gabor analysis: extraction of instantaneous frequencies. IEEE Trans Inf Theory 38:644–664
10. Forte JD, Bui BV, Vingrys AJ (2008) Wavelet analysis reveals dynamics of rat oscillatory potentials. J Neurosci Methods 169:191–200
11. Fortune B, Bearse MA, Cioffi GA, Johnson CA (2002) Selective loss of an oscillatory component from temporal retinal multifocal ERG responses in glaucoma. Invest Ophthalmol Vis Sci 43:2638–2647
12. Frishman LJ, Saszik S, Harwerth RS et al (2000) Effects of experimental glaucoma in macaques on the multifocal ERG: multifocal ERG in laser-induced glaucoma. Doc Ophthalmol Adv Ophthalmol 100:231–251
13. Graham SL, Klistorner AI, Grigg JR, Billson FA (2000) Objective VEP perimetry in glaucoma: asymmetry analysis to identify early deficits. J Glaucoma 9:10–19
14. Harwerth RS, Crawford ML, Frishman LJ, Viswanathan S, Smith EL, Carter-Dawson L (2002) Visual field defects and neural losses from experimental glaucoma. Prog Retin Eye Res 21:91–125
15. Ho WC, Wong OY, Chan YC, Wong SW, Kee CS, Chan HH (2012) Sign-dependent changes in retinal electrical activity with positive and negative defocus in the human eye. Vis Res 52:47–53
16. Holder GE (2001) Pattern electroretinography (PERG) and an integrated approach to visual pathway diagnosis. Prog Retin Eye Res 20:531–561
17. Hood DC, Greenstein VC, Holopigian K et al (2000) An attempt to detect glaucomatous damage to the inner retina with the multifocal ERG. Invest Ophthalmol Vis Sci 41:1570–1579
18. Hood DC, Odel JG, Chen CS, Winn BJ (2003) The multifocal electroretinogram (ERG): applications and limitations in neuro-ophthalmology. J Neuroophthalmol 23:225–235
19. Hood DC, Zhang X (2000) Multifocal ERG and VEP responses and visual fields: comparing disease-related changes. Doc Ophthalmol 100:115–137
20. Hori N, Komori S, Yamada H, Sawada A, Nomura Y, Mochizuki K, Yamamoto T (2012) Assessment of macular function of glaucomatous eyes by multifocal electroretinograms. Doc Ophthalmol Adv Ophthalmol 125:235–247
21. Kook MS, Sung K, Kim S, Park R, Wang W (2001) Study of retinal nerve fiber layer thickness in eyes with high tension glaucoma and hemifield defect. Br J Ophthalmol 85:1167–1170
22. Kumar R, Indrayan A (2011) Receiver operating characteristic (ROC) curve for medical researchers. Indian Pediatr 48:277–281
23. Ledolter AA, Kramer SA, Todorova MG, Schötzau A, Palmowski-Wolf AM (2013) The effect of filtering on the two-global-flash mfERG: identifying the optimal range of frequency for detecting glaucomatous retinal dysfunction. Doc Ophthalmol 126:117–123
24. Luo X, Patel NB, Harwerth RS, Frishman LJ (2011) Loss of the low-frequency component of the global-flash multifocal electroretinogram in primate eyes with experimental glaucoma. Invest Ophthalmol Vis Sci 52:3792–3804
25. Medeiros FA, Zangwill LM, Bowd C, Weinreb RN (2004) Comparison of the Gdx VCC scanning laser polarimeter, HRT II confocal scanning laser ophthalmoscope, and stratus OCT optical coherence tomograph for the detection of glaucoma. Arch Ophthalmol 122:827–837
26. Miguel-Jiménez JM, Boquete L, Ortega S, Rodríguez-Ascariz JM, Blanco R (2010) Glaucoma detection by wavelet-based analysis of the global flash multifocal electroretinogram. Med Eng Phys 32:617–622
27. Miguel-Jiménez JM, Ortega S, Boquete L, Rodríguez-Ascariz JM, Blanco R (2011) Multifocal ERG wavelet packet decomposition applied to glaucoma diagnosis. Biomed Eng Online 10:37
28. Palmowski-Wolfe AM, Todorova MG, Orgül S (2011) Multifocal oscillatory potentials in the 'two global flash' mfERG in high and normal tension primary open-angle glaucoma. J Clin Exp Ophthalmol 2:167. doi:10.4172/2155-9570.1000167
29. Rangaswamy NV, Hood DC, Frishman LJ (2003) Regional variations in local contributions to the primate photopic flash ERG: revealed using the slow-sequence mfERG. Invest Ophthalmol Vis Sci 44:3233–3247
30. Sainani K (2010) The importance of accounting for correlated observations. PM & R J Inj Funct Rehabil 2(9):858–861. doi:10.1016/j.pmrj.2010.07.482
31. Shimada Y, Li Y, Bearse MA, Sutter EE, Fung W (2001) Assessment of early retinal changes in diabetes using a new multifocal ERG protocol. Br J Ophthalmol 85:414–419
32. Sutter EE, Tran D (1992) The field topography of ERG components in man. I. The photopic luminance response. Vis Res 32:433–446
33. Sutter EE, Bearse MA (1999) The optic nerve head component of the human ERG. Vis Res 39:419–436
34. Todorova MG, Palmowski-Wolfe AM (2011) MfERG responses to long-duration white stimuli in glaucoma patients. Doc Ophthalmol Adv Ophthalmol 122:87–97
35. Wu LL, Suzuki Y, Kunimatsu S, Araie M, Iwase A, Tomita G (2001) Frequency doubling technology and confocal scanning ophthalmoscopic optic disc analysis in open-angle glaucoma with hemifield defect. J Glaucoma 10:256–260
36. Wu Y, Wang H, Zhang B, Du KL (2012) Using radial basis function networks for function approximation and classification. ISRN Appl Math 2012:324194. doi:10.5402/2012/324194